LBL-25090 c.2
UC-210

Lawrence Berkeley Laboratory
UNIVERSITY OF CALIFORNIA

RECEIVED
LAWRENCE
BERKELEY LABORATORY
JUN 9 1988
LIBRARY AND
DOCUMENTS SECTION

APPLIED SCIENCE DIVISION

Spectroscopic Studies of the Passive Film on Alkali and Alkaline Earth Metals in Non-Aqueous Solvents– A Surface Science Approach: Final Report

P. Herrera-Fierro, X. Xing, G. Chottiner, and D.A. Scherson

April 1988

TWO-WEEK LOAN COPY
This is a Library Circulating Copy which may be borrowed for two weeks.

APPLIED SCIENCE DIVISION

Prepared for the U.S. Department of Energy under Contract Number DE-AC03-76SF00098.

LBL-25090 c.2

DISCLAIMER

This document was prepared as an account of work sponsored by the United States Government. While this document is believed to contain correct information, neither the United States Government nor any agency thereof, nor the Regents of the University of California, nor any of their employees, makes any warranty, express or implied, or assumes any legal responsibility for the accuracy, completeness, or usefulness of any information, apparatus, product, or process disclosed, or represents that its use would not infringe privately owned rights. Reference herein to any specific commercial product, process, or service by its trade name, trademark, manufacturer, or otherwise, does not necessarily constitute or imply its endorsement, recommendation, or favoring by the United States Government or any agency thereof, or the Regents of the University of California. The views and opinions of authors expressed herein do not necessarily state or reflect those of the United States Government or any agency thereof or the Regents of the University of California.

LBL-25090

SPECTROSCOPIC STUDIES OF THE PASSIVE FILM ON ALKALI AND ALKALINE EARTH METALS IN NON-AQUEOUS SOLVENTS: A SURFACE SCIENCE APPROACH

Final Report

April 1988

by

Pilar Herrera-Fierro
Xuekun Xing
Gary Chottiner
Daniel A. Scherson

Case Center for Electrochemical Sciences and
the Departments of Chemistry and Physics
Case Western Reserve University
Cleveland, Ohio 44106

for

Technology Base Research Project
Applied Science Division
Lawrence Berkeley Laboratory
University of California
Berkeley, California 94720

This work was supported by the Assistant Secretary for Conservation and Renewable Energy, Office of Energy Storage and Distribution of the U.S. Department of Energy under Contract No. DE-AC03-76SF00098, Subcontract No. 4528410 with the Lawrence Berkeley Laboratory.

TABLE OF CONTENTS

I. INTRODUCTION 1

II. INSTRUMENTAL ASPECTS 1

A. Thermal Desorption 1
B. Variable Temperature Sample Holder 1
C. UHV-Electrochemical Cell Transfer System 1

III. EXPERIMENTAL ASPECTS 4

IV. RESULTS AND DISCUSSION 5

A. Bonding and Reactivity of O_2, CO and CO_2 on Bare and K Covered Ag(111) Surfaces 5
1. Dioxygen 5
2. Carbon Monoxide 6
3. Carbon Dioxide 7
B. The Single Crystal Metal Non-Aqueous Solvent Interface: Fundamental Studies 9
1. Cyclic Voltammetry and Differential Capacity Curves for Ag(111) and Au(111) in Tetra n-butyl Ammonium Perchlorate Propylene Carbonate Solutions 9
2. Reactivity of Ag(111) and Au(111) in $LiClO_4$/PC Solutions 11

V. REFERENCES 13

VI. TABLE I 15

VII. FIGURE CAPTIONS 16

I. INTRODUCTION

Most of the effort during this past year was focused on two areas:

i) the acquisition of detailed information regarding the adsorption of O_2, CO and CO_2 on K covered Ag(111) surfaces, and

ii) a cyclic voltammetric study of Ag(111) and Au(111) in tetraalkyl ammonium perchlorate- and $LiClO_4$-propylene carbonate solutions.

This report summarizes the progress made in each of these areas as well as the present status of the instrumental array involved in the ultra high vacuum(UHV)-electrochemical cell experiments.

II. INSTRUMENTAL ASPECTS

A. Thermal Desorption Spectroscopy

The thermal desorption spectroscopy (TDS) unit has become fully operational. The actual heating of the specimens is currently being conducted manually, but the data acquisition and processing are completely computerized using ASYST-based software. Work is now in progress to finalize the construction and testing of the voltage-controlled phase controller that interfaces the OMEGA temperature controller and the sample heater. After completion of this step the operation of the TDS unit will be fully automatic.

B. Variable Temperature Sample Holder

An improved cold finger was designed and constructed to fit a new differentially pumped rotary feedthrough (UHV Instruments) and XYZ precision manipulator (Huntington). This new arrangement enables a much faster cooling rate and a better degree of reproducibility in the positioning of samples during the experiments, compared to the old unit.

C. UHV-Electrochemical Cell Transfer System

The design and construction of the UHV-electrochemical cell transfer system has essentially been completed, and preliminary tests have yielded

excellent results. A schematic diagram of the unit is shown in Fig. 1. It consists of an independently pumped auxiliary UHV chamber, connected via a gate valve to the main chamber that houses the electron-based spectroscopies. Samples are introduced and retrieved from the main and auxiliary chambers by means of a transfer-tilt mechanism. All the components involved in the preparation of the electrochemical cell are located in an all-stainless-steel arm with a magnetically coupled manipulator which is attached via a gate valve to the auxiliary chamber. This is shown schematically in Fig. 2.

The electrochemical cell to be used in aqueous media consists of a Teflon block with three interconnected cylindrical orifices (see B, Fig. 3). The counter electrode, made of an appropriate material, is cast in Kel-F and then press fitted into the largest diameter orifice centered along the main axis of the manipulator rod onto which the block is attached. Two smaller orifices were drilled at an equal distance from the center of the rod and connected to each other by a fine drilled-in capillary (not shown in the figure). A platinum wire is inserted in each of these holes and then used as the components of a dynamic reference electrode. A fine hole (not shown in the figure) was also drilled into the Kel-F block to connect the hydrogen side of the dynamic reference electrode to the counter electrode compartment and thus serve as a Luggin capillary.

In the case of non-aqueous solvents, the reference electrode compartment will be isolated from the working electrode cavity by means of a platinum crack-seal. This is made by melting glass around a fine platinum wire and allowing the junction to cool down. Because of the differences in the thermal expansion coefficients, a microscopic crack develops at the glass-metal interface. Upon exposure to the electrolyte, a very small amount

of solution fills the crack allowing electrolytic contact to be established with a negligible rate of leakage across the length of the crack.

The electrolyte management system enables both the introduction and removal of liquids to and from the electrochemical cell. The delivery section (see A, Fig. 3) consists of an all-Teflon vessel, in which the electrolyte is stored and deaerated, connected to a three-way right angle valve. In one of the valve positions, a small volume of electrolyte can be withdrawn from the container by means of a syringe. The valve is then rotated by ninety degrees and the liquid in the syringe is delivered onto the counter electrode and then into the reference electrode compartments after an appropriate translation of the main manipulator. The gate valve that connects the electrochemical arm to the auxiliary chamber is then opened and the cell transferred to a point directly below the single crystal to be examined. The vertical manipulator is then lowered until the electrolyte contacts the working electrode for electrochemical measurements. After the experiment is completed, the cell is taken apart by simply raising the vertical manipulator. One of the approaches employed to remove the excess electrolyte that almost invariably remains adhered to the electrode surface after emersion will be to touch the drop surface with a piece of high-purity filter paper attached to the end of the Teflon block. If necessary, the working electrode can be tilted to force the last traces of bulk electrolyte adhered to the surface to flow downwards towards the edge of the crystal where it is removed by contact with the piece of paper.

As mentioned earlier, the electrolyte management system also has provisions for removing the electrolyte after each experiment (see B, Fig. 3). This is effected with a Teflon tube inserted into an L-shaped stainless steel arm attached to the side of a double-sided flange which can rotate about an axis perpendicular to the plane of the cell. In this fashion, the

tip of the tube is inserted into each of the orifices to remove traces of trapped electrolyte. This is a very convenient arrangement to avoid opening the cell preparation compartment to the atmosphere between experiments.

At the time of preparation of this report the auxiliary chamber and electrochemical arm were being installed in the main UHV system.

III. EXPERIMENTAL ASPECTS

Except where otherwise indicated all experiments were conducted with a Ag(111) single crystal obtained from Metron Inc., New Jersey. Prior to its introduction into the UHV chamber, the crystal was oriented and cut by spark erosion according to procedures specified in detail elsewhere. Once in the UHV chamber the Ag(111) crystal was subjected to a series of Ar^+ sputtering-annealing cycles until excellent LEED patterns and AES spectra were obtained. The potassium layer was deposited by the same methodology described in earlier reports. To the level of sensitivity of AES, the potassium were found to be free of O and C contamination. An increase in the overall background intensity without the appearance of extra spots was observed in the LEED patterns upon deposition of 30% of a monolayer of K on Ag(111); this provides some evidence that the potassium atoms are either randomly distributed on the substrate surface or have too high a mobility to generate ordered structures (at room temperature). No changes in the LEED or AES were observed after annealing the Ag/K surface for 5 min, which indicates that at this temperature there is no evaporation of the alkali metal nor diffusion into the silver. At 40% coverage, the background intensity was so high that the spots associated with the substrate were barely seen. It is interesting to note that some variations in the relative intensities of the K and Ag AES peaks were noted as a function of the sample position with respect to the electron beam immediately after deposition of

the alkali metal. After mild annealing, however, the peaks disappeared, indicating that such heat treatment promotes a more even distribution of K on the silver surface.

IV. RESULTS AND DISCUSSION

A. Bonding and Reactivity of O_2, CO and CO_2 on Bare and K-Covered Ag(111) Surfaces.

Ag(111) has been found to exhibit little if any affinity for any of the non-aqueous solvents examined and therefore the effects observed may be attributed solely to the presence of submonolayer coverages of K on the surface. Dioxygen, carbon monoxide and carbon dioxide have been selected for these studies, because they are the most likely products of the alkali-metal induced decomposition of various non-aqueous solvents.

A.1 Dioxygen

Oxygen was found to adsorb at -186°C on Ag(111), yielding a (1 X 1) LEED pattern. The change in work function associated with the exposure of bare Ag(111) at that temperature to 180 L of O_2 was about +1.2 V. Despite the presence of some form of oxygen bound to the silver surface, the O-AES peak at 511 eV was not detected. This phenomenon may be attributed to a beam-induced desorption of the physisorbed O_2. The TDS of a clean, cold (-186°C) Ag(111) surface showed no peaks for the five monitored masses, i.e. 16, 28, 32, 39, 44. The same surface dosed with 180 L of O_2, however, yielded a spectra with a single peak at mass 44 (see Fig. 4). This can be attributed to a thermally induced reaction between adsorbed oxygen and background CO. It may be noted that the dosing of O_2 was performed for 180 s at $1 \cdot 10^{-6}$ torr. The time required to form a monolayer on the surface at a pressure of $5 \cdot 10^{-10}$ torr is 1800 s. Therefore, it is conceivable that a monolayer of CO may have reacted during this time with O_2 on the surface. This process has been reported for a number of other surfaces.[1-4] Adsorbed

oxygen was also found to induce the adsorption of CO_2 on Ag(111), a species that exhibits no affinity for bare Ag(111) down to -186°C. This reaction was followed by work function measurements and also by the disappearance of the (1 X 1) LEED pattern while admitting CO_2 into the chamber.

The presence of K on the Ag(111) surface significantly increased the sticking coefficient of O_2 on Ag(111). Fig. 5 shows the AES spectra of a surface containing about 30 % of vapor-deposited K which was later exposed to saturation coverages of O_2. The TDS spectra of this surface for masses 32 (Curve a), 28 (Curve b) and 44 (Curve c) is given in Fig. 6. The peak corresponding to potassium could not be detected. Based on the quantitative analysis of the fragmentation pattern, the CO originates solely from the decomposition of CO_2 in the mass spectrometer and not from the sample. Kitson et al.[5] have also studied the O_2/K/Ag(111) system and reported TDS peaks at 600 K and 870 K, which varied as a function of K coverage and O_2 exposure. In view of these results, and the absence of clearly defined clear LEED patterns it may suggested that the reaction of O_2 with K/Ag(111) surfaces yields an amorphous layer of some form of potassium oxide.

A.2 Carbon Monoxide

This system was examined in order to gain insight into the alkali-metal-induced activation of CO_2. The adsorption of CO on K-covered surfaces has been studied by other workers, thus providing an ideal means for a quantitative assessment of the operation of the UHV instrumental array. Fig. 7 shows the AES spectra of a surface prepared by dosing CO to saturation on a K/Ag(111) substrate at room temperature. The change in work function was about -2.2 V. Similar experiments conducted in the absence of K on the surface indicated that CO does not adsorbed on Ag(111) at 290 K. The alkali-metal-induced adsorption of CO is consistent with the presence of the oxygen

peak in the AES spectra and the change in work function as monitored **in situ** during admission of CO into the chamber.

Only one desorption peak was observed in the TDS spectra for high coverages of K and saturation exposure to CO (see Fig. 8), in direct analogy with the results obtained for the better known CO/K/Ni(111) system. A comparison of the peak desorption temperature obtain in these experiments with those reported by other workers is given in Table I.

No evidence for oxygen desorption was observed in the TDS spectra. Furthermore, AES analysis after TDS failed to reveal oxygen on the surface. This is in accordance with the widely accepted view that CO dissociates on the Ag surface and then undergoes recombination during the thermally activated desorption, as demonstrated by Ng et al.[6] in their isotope mixing experiments.

A CO_2 desorption peak that has not been reported in earlier work was seen during the CO-TDS experiments. A similar phenomenon was observed by Madden and Ertl[7] in their studies involving CO-TDS from Ni(110). These authors suggested that CO_2 is formed on the surface via an electron- beam-induced disproportionation of CO at temperatures in the range between 500 and 1000 K. It thus seems reasonable to assume that K may also be capable of promoting CO dissociation. Unfortunately carbon is very difficult to detect by AES because the 272 eV peak overlaps with the Ag 266 eV peak.

A.3. Carbon Dioxide

Among the small molecules selected for these studies, CO_2 appears particularly interesting, as it is believed to be one of the major decomposition products of propylene carbonate, a solvent proposed for battery applications. Furthermore, the interactions of CO_2 with alkali metals have been investigated rather extensively by matrix isolation techniques, providing a framework for a comparison with UHV experiments of

the type involved in this project.

The results obtained may be summarized as follows:

i) Carbon dioxide does not adsorb on clean Ag(111) even at temperatures as low as -186°C. This conclusion is based on **in situ** work function ($\Delta\phi$) and AES measurements for which no changes were observed in the values of $\Delta\phi$, and no carbon or oxygen is detected after long exposure of the silver single crystal to CO_2.

ii) No extra diffraction spots were observed upon depositing potassium at submonolayer coverages on the Ag(111) surface even after annealing up to temperatures of 400°C. This behavior is unlike that found in the case of K on Ni(111) where an ordered superlattice was clearly identified.

iii) About a monolayer of K deposited on Ag(111) gives rise to a change in work function of about -2.5 eV. This corresponds to a surface composition of 18% as determined from the relative intensities of the AES peaks.

iv) The maximum change in work function induced by the adsorption of CO_2 to saturation coverages on a potassium-covered Ag(111) was approximately +0.8 V. This is consistent with a partial charge transfer from the surface to the CO_2-LUMO, an effect that is expected to be accompanied by a bending of the otherwise linear O=C=O molecule.

v) Four major peaks at temperatures of 400(I), 500-600(II), 770 and 840K were detected in the thermal desorption spectra of CO_2 adsorbed on K-covered Ag(111) surfaces. The relative heights of peaks III and IV depend on the ratio of K to CO_2 coverage. In particular, peak III became more prominent in excess potassium, whereas peak IV dominated when the ratio was inverted. This is illustrated in Figs. 9 through 11.

It seems conceivable that peaks I and II are associated with single CO_2 molecules coordinated to potassium atoms on the surface in two different

configurations, whereas the peaks observed at higher temperatures may involve interaction between the adsorbed CO_2 molecules to yield oxalate-type structures formed via a radical coupling mechanism. Similar species have been proposed in the case of codeposition of Li or Na and CO_2 in Ar matrices at low temperatures, on the basis of infrared spectroscopy results. It is interesting to note that LiC_2O_4 could only be detected in very concentrated matrices.

B. The single crystal metal non-aqueous solvent interface: Fundamental Studies

Considerable insight into the reactivity of metal surfaces in propylene carbonate solutions was obtained from a series of voltammetric studies involving tetra alkyl ammonium perchlorate and $LiCO_4$ electrolytes.

B.1. Cyclic Voltammetry and Differential Capacity Curves for Ag(111) and Au(111) in Tetra n-butyl Ammonium Perchlorate (TBAP) Propylene Carbonate (PC) Solutions.

The cyclic voltammograms of Ag(111) in a 0.1 M TBAP/PC solution are given in Fig. 12. Two current-potential peaks were observed between 2.0 and 2.2 V in the first scan in the negative direction, which merged into a single peak in subsequent sweeps. The peak observed at 2.2 V, in the first scan may be due to the reduction of adventitious impurities, which as judged by its magnitude are present in very small amounts. The peak at ~2.0 V vs. Li/Li^+ is most likely associated with a double-layer phenomenon involving ionic specific adsorption and/or the inner Helmholtz layer.

Fig. 13 shows capacity vs potential (C vs E) curves obtained for a Ag(111) electrode in the same electrolyte. A minimum in the C vs. E curve C_{min}, was found at a potential of ~ 2.2 V vs Li/Li^+ which was practically independent of the electrolyte concentrations that were examined. The values of C_{min} are 7 to 9 $\mu F/cm^2$ which are smaller than those found normally

in aqueous media, but comparable to those in non-aqueous solutions reported by other authors.[12-21]

In the case of Au(111), the C vs E curve in 0.01 M TBAP/PC solution exhibited a minimum at about 3.4 V vs. Li/0.1 M Li^+, with C_{min} of about $5.7\mu F \cdot cm^{-2}$ (see Fig. 14.). van Huong examined the C vs E curves for the main three low index planes of gold in PC electrolytes .[21] Although the magnitude of the capacity was similar to that reported in this work, the overall shape of the curves was found to be essentially independent of the crystal plane exposed to the electrolyte.

Several interesting observations can be made on the basis of the results obtained:

i) The potential difference between the two maxima in the C vs E curve for Ag(111) in 0.01 M TBAP/PC (2.0 and 2.5 V vs Li/Li^+) is about 0.5 V, which is almost identical to that observed in NaF aqueous solutions in this and other laboratories.[22,23]

ii) The difference in the point of zero charge (pzc) between Ag(111) and Au(111) in aqueous solutions containing ions which do not exhibit specific adsorption is about 1.05 V.[23] This is slightly smaller, but nevertheless comparable to the pzc (1.2 V) observed in propylene carbonate.

iii) The pzc for polycrystalline gold in 0.1 M $NaClO_4$/PC is reported to be about -0.5 V vs Ag/0.01M Ag^+,PC.[20] Based on a direct measurement of the potential of this reference electrode versus that of an aqueous mercury mercuric sulfate (MSE), without correcting for the liquid junction potential, van Houng estimated that the pzc for polycrystalline Au in PC is about -0.24 vs MSE, which corresponds to 0.16 V vs SCE. This value is about 0.20 V more positive than that reported in water.[24,25] The E_{min} for Ag(111) in TBAP/PC was found to be of about 2.20 V vs Li/0.01M Li^+ which corresponds to -1.22 V vs Ag/0.01M Ag^+,PC. The difference in potential

between the two reference electrodes was determined using the experimental value of Li bulk deposition as a reference yielding $E_{Li/0.1\underline{M}\ Li^+} = -3.42$ V vs Ag/0.01$\underline{M}$ Ag^+,PC. Based on van Houng's arguments this value would be of about -0.56 V vs SCE, which is 0.16 V more positive that the pzc of Ag(111) in aqueous media (-0.72 V vs SCE).[23] If this type of calculation is applied to the data of Parsons et al.[16] and Payne et al.[17] for mercury in propylene carbonate, the shift also amounts to 0.13-0.14 V. In the case of Au(111) the shift is also positive although much larger than that observed for Ag(111).

B.2. Reactivity of Ag(111) and Au(111) in $LiClO_4$/PC solutions

The cyclic voltammetry and C vs E curves of Ag(111) obtained in $LiClO_4$/PC solutions are qualitatively similar to those in TBAP, provided the potential range is not extended beyond 1.4 V (see Figs. 15 and Fig. 16a). From a quantitative viewpoint, however, two differences are worth noting:

i) C_{min}, 15μF/cm^2, is larger than that found in TBAP although it is still smaller than those in the aqueous media. The reasons which may account for these observations are not clear, but would probably be associated with the properties of the Li^+ cation, an extremely small ion.

ii) The potential associated with C_{min} is about 2.30 V, and thus slightly more positive than that in TBAP.

As was reported in a previous communication,[27] the onset of a large irreversible cathodic peak without an anodic counterpart was found at about ~1.4 V during the first cycle in the negative direction. This cathodic peak gradually disappeared in subsequent scans (see Fig. 15). The C vs. E curves obtained with a fresh electrode and one that was cycled in the region of the cathodic peak were significantly different (see Fig. 16a and b). In particular the latter yielded an essentially featureless curve with a much

smaller overall capacitance. This provides evidence for a dramatic change in the surface properties. It was previously suggested that this could be due to the formation of a film on the electrode surface produced by the reaction of adventitious impurities in the electrolyte. For example, hydroxyl ions could be produced during the reduction of water and yield a highly insoluble species such as LiOH.

The results of essentially identical experiments with Au(111) electrodes are shown in Fig. 17. As was the case with Ag(111) in $LiClO_4$/PC solutions, a large current was observed in the scan in the negative direction at a potential of about 1.9 V vs Li/Li^+, and thus ~0.5 V more positive than that observed for Ag(111). On the basis of these new results, it may be proposed that the reaction responsible for the large negative currents is not the reduction of impurities, but rather the decomposition of the solvent[26] which is catalyzed by the underpotential-deposited Li [Li(UPD)] ad-atoms on the substrate surface. This reaction is schematically represented as follows:

$$Li^+ + e^- \longrightarrow Li(UPD)$$

$$Li(UPD) + PC \longrightarrow Li(PC')$$

in which Li(PC') denotes the reaction product of PC decomposition.

According to this proposed model, this process would create a blocking layer that would be responsible for the observed distortions in the differential capacitance curves. This interpretation is supported by the fact that because of the very large work function difference, Li(UPD) would be expected to occur at very positive potentials on Au and Ag and more positive than in the case of Au(111) than Ag(111).

Thus, is concluded that the reactivity of Li ad-atoms is extremely high, leading to the decomposition of propylene carbonate at potentials far more positive than those associated with the bulk deposition of the alkali

metal.

V. REFERENCES

1. T. E. Felter, W. H. Weinberg, G. Ya. Lastuhkina, A. I. Boronin, P. A. Zhdan, G. K. Boreskov and J. Hrbek, Surface Science, 118 (1982) 369.

2. T. E. Felter, W. H. Weinberg, P. A. Zhdan and G. K. Boreskov, J. Vac. Sci. Technol., 18 (1981) 622.

3. T. E. Felter, W. H. Weinberg, G. Ya. Lastuhkina, P. A. Zhdan, G. K. Boreskov and J. Hrbek, Applications of Surface Science, 16 (1983) 357.

4. G. Rovida, F. Pratesi, M. Maghetta and E. Ferroni, Surface Science, 43 (1974) 230.

5. M. Kitson and M. Lambert, Surface Science, 109 (1981) 60.

6. L. Ng, K. J. Uram, Z. Xy, P. L. Jones and J. T. Yates, J. Chem. Phys., 86 (1987) 6523.

7. H. H. Madden and G. Ertl, Surface Science, 35 (1973) 211.

8. Jiwha Lee, J. Arias, C. P. Hanrahan, R. M. Martin and H. Metiu, J. Chem. Phys., 82 (1985) 485.

9. A. Berko and F. Solymosi, Surface Science, 171 (1986) L498.

10. J. E. Crowell and G. A. Somorjai, Applications of Surface Science, 19 (1984) 73.

11. J. E. Crowell, E. L. Garfunkel and G. A. Somorjai, Surface Science, 121 (1982) 303.

12. O. A. Petrii, I.G. Khomchenko and A. G. Zelinskii, Elektrokhimiya, 15 (1979) 400.

13. E. Yu Alekseeva, V.A. Safonov and O.A. Petrii, Elektrokhimiya, 20 (1984) 945.

14. W.R.Fawcett and R.O. Loutfy, Can. J. Chem., 51 (1973) 230.

15. W.R.Fawcett and R.O. Loutfy, J. Electroanal. Chem., 39 (1972) 185.

16. T. Biegler and R. Parsons, J. Electroanal. Chem., 21 (1969) App.4.

17. R. Payne, J. Phys. Chem., 71 (1967) 1548.

18. R. Payne, J. Phys. Chem., 73 (1969) 3598.

19. R. Gambert and H. Baumgaertel, J. Electroanal. Chem., 183 (1985) 315.

20. C.N. van Houng, J. Electroanal. Chem., 194 (1985) 131.

21. C.N. van Houng, J. Electroanal. Chem., 207 (1986) 235.

22. G. Valette, A. Hamelin and R. Parsons, Z. Phys. Chem., N.F., 113 (1978) 71.

23. A. Hamelin, T. Vitanov, E. Sevastyanov and A. Popov, J. Electroanal. Chem., 145 (1983) 225.

24. J. Clavilier and C. N. van Huong, J. Electroanal. Chem., 80 (1977) 101.

25. C. Hinnen, C.N. van Houng, A. Rousseau and J.P. Dalbera, J. Electroanal. Chem., 95 (1979) 131.

26. M. Arakawa and J.I. Yamaki, J. Electroanal. Chem., 219 (1987) 273.

27. X. Xing, P. Abel, R. McIntyre and D. Scherson, J. Electroanal. Chem., 216 (1987) 261.

VI. TABLE I

Thermal Desorption Peak Temperature T_p, for CO Adsorbed on Potassium Covered Single Crystal Surfaces

System	T_p, K	Reference
K/Ag(111)	824	This Work
K/Ni(111)	630	Ng et al.[6]
K/Ni(111)	640	Lee et al.[8]
K/Pd(100)	610	Berko et al.[9]
K/Rh(111)	700	Crowell et al.[10]
K/Pt(111)	600	Crowell et al.[11]

VII. FIGURE CAPTIONS

Fig. 1. Schematic diagram of the UHV-electrochemical system.

Fig. 2. Schematic diagram of the electrochemical arm and auxiliary ultra high vacuum chamber.

Fig. 3. Schematic diagram of electrolyte management system. A. Delivery, B. Removal.

Fig. 4. Mass 44 TDS of 180 L of O_2 adsorbed on Ag(111) at -186°C. Heating Rate = 4.3 $K \cdot s^{-1}$.

Fig. 5. AES of surface containing 27% K and 10% oxygen.

Fig. 6. TDS spectra of surface described in caption Fig. 5. a. Mass 32, b. Mass 28 and c. Mass 44.

Fig. 7. AES of K/Ag(111) surface dosed with 200 L CO.

Fig. 8. CO-TDS of surface described in caption Fig. 7.

Fig. 9. Thermal desorption spectra of a surface containing 14% K exposed to 0.5 L CO_2. Heating rate: 6 $K \cdot s^{-1}$.

Fig. 10. Thermal desorption spectra of a surface containing 18% K exposed to 60 L CO_2. Heating rate: 6 $K \cdot s^{-1}$.

Fig. 11. Thermal desorption spectra of a surface containing 9% K exposed to 0.25 L CO_2. Heating rate: 6 $K \cdot s^{-1}$.

Fig. 12. Cyclic voltammogram of Ag(111) in 2mM TBAP/PC solution. ν = 10 $mV \cdot s^{-1}$. ------: first cycle, _____: subsequent cycles

Fig. 13. C vs. E curves for Ag(111) in TBAP/PC solutions: a. 8mM; b. 10mM; c. 50mM. ν = 5 $mV \cdot s^{-1}$. AC signal: Amplitude = 5 mV, f = 40 Hz.

Fig. 14. C vs. E curves for Au(111) in 0.01 M TBAP/PC solution. ν = 10 $mV \cdot s^{-1}$. AC signal: Amplitude = 5 mV, f = 20 Hz.

Fig. 15. Cyclic voltammogram of Ag(111) in 0.1 M $LiClO_4$/PC solution. ν = 10 $mV \cdot s^{-1}$. 1. first, 2. second, and 3. third cycle.

Fig. 16. C vs. E curves for Ag(111) in 50 mM $LiClO_4$ solution, before (a) and after (b) excursion to negative region (0.8 V vs Li/Li^+)

Fig. 17. Cyclic voltammogram of Au(111) in PC solution containing:
a. 0.01 M TBAP
b. 0.01 M $LiClO_4$
ν = 10 $mV \cdot s^{-1}$. Number represents the cycle sequence.

Fig. 18. C vs. E curves for Au(111) in 0.01 M $LiClO_4$/PC solution. ν = 10 $mV \cdot s^{-1}$. AC signal: Amplitude = 5 mV, f = 20 Hz.

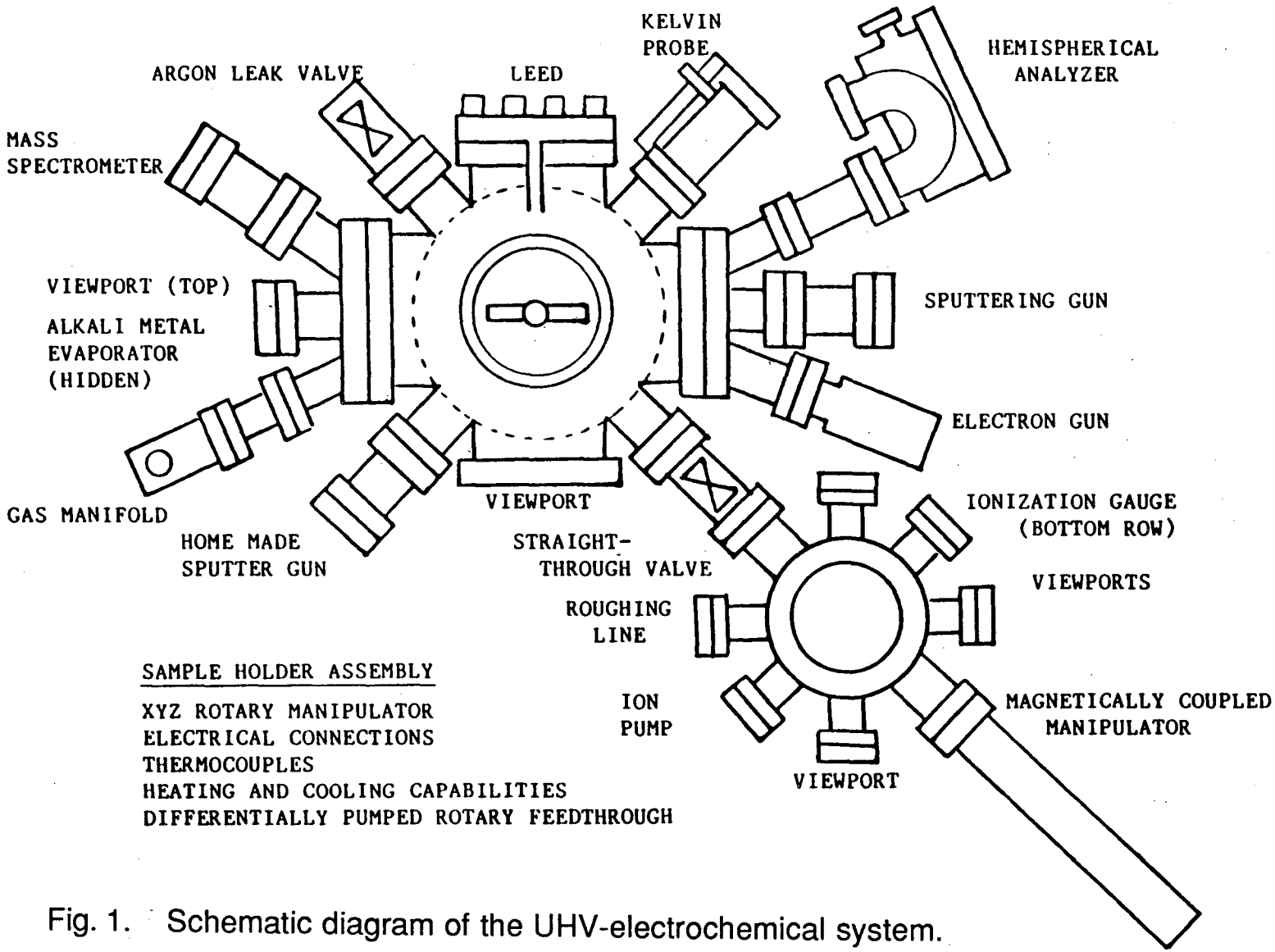

Fig. 1. Schematic diagram of the UHV-electrochemical system.

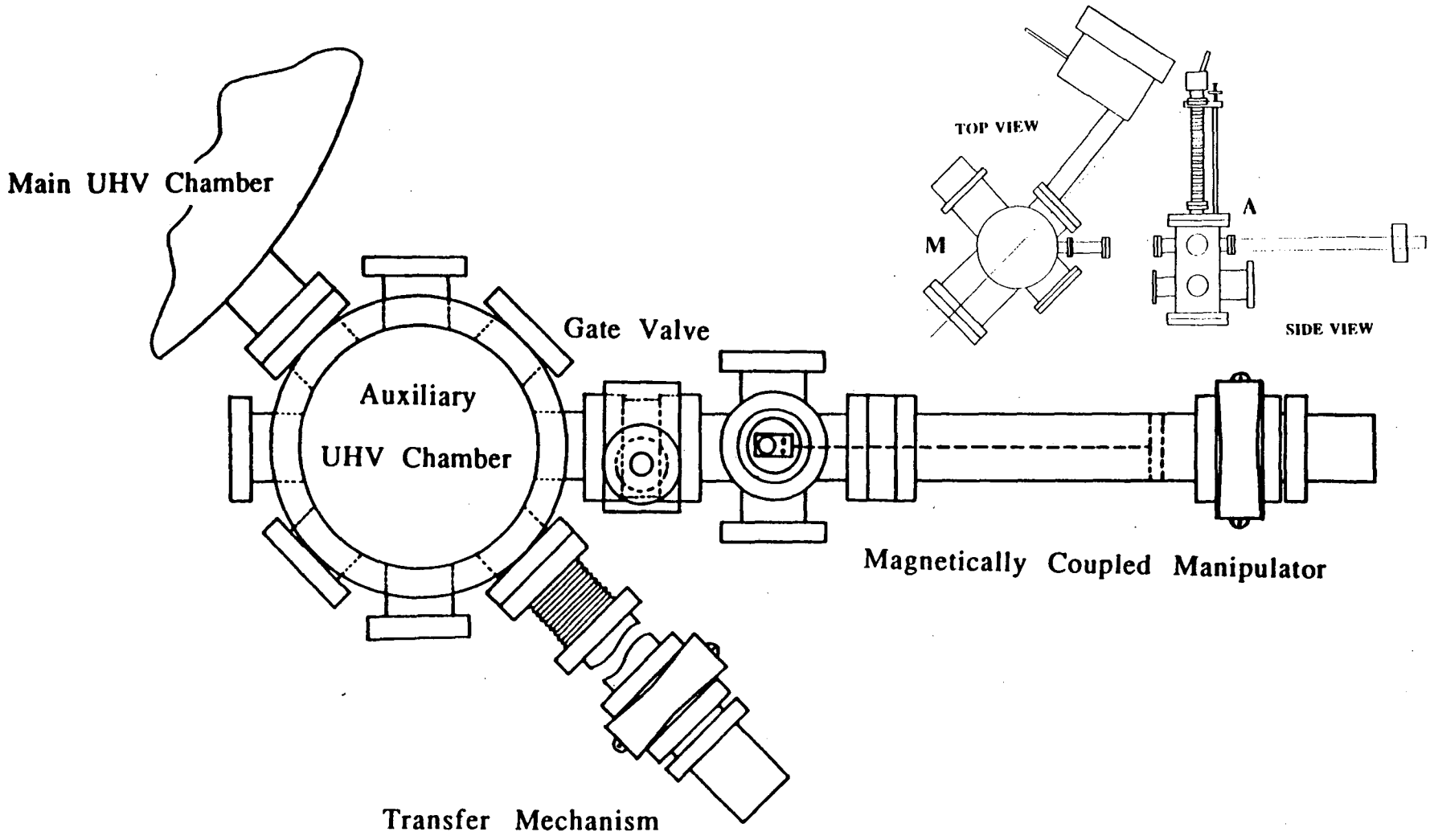

Fig. 2. Schematic diagram of the electrochemical arm and auxiliary ultra high vacuum chamber.

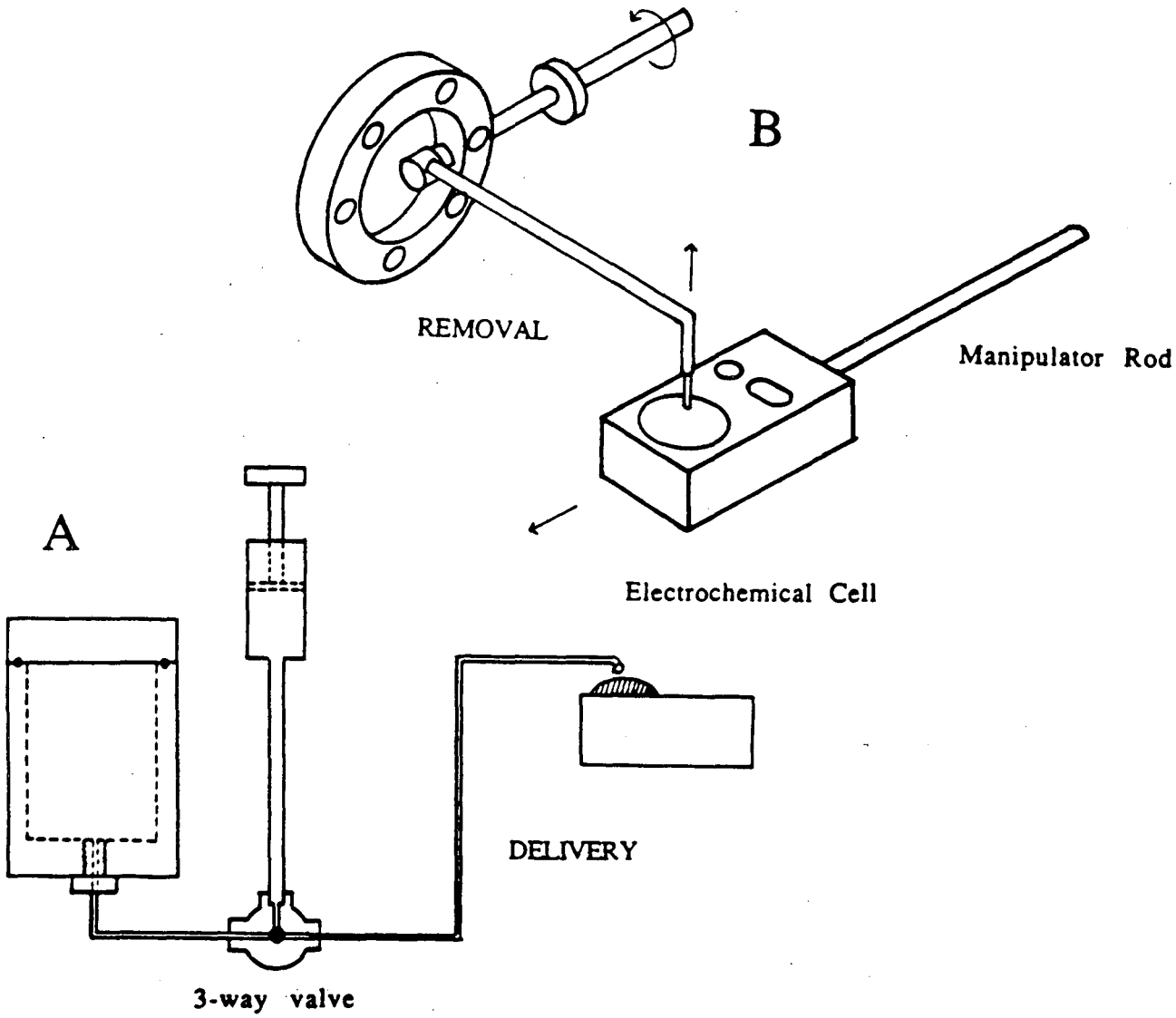

Fig. 3. Schematic diagram of electrolyte management system.
A. Delivery; B. Removal.

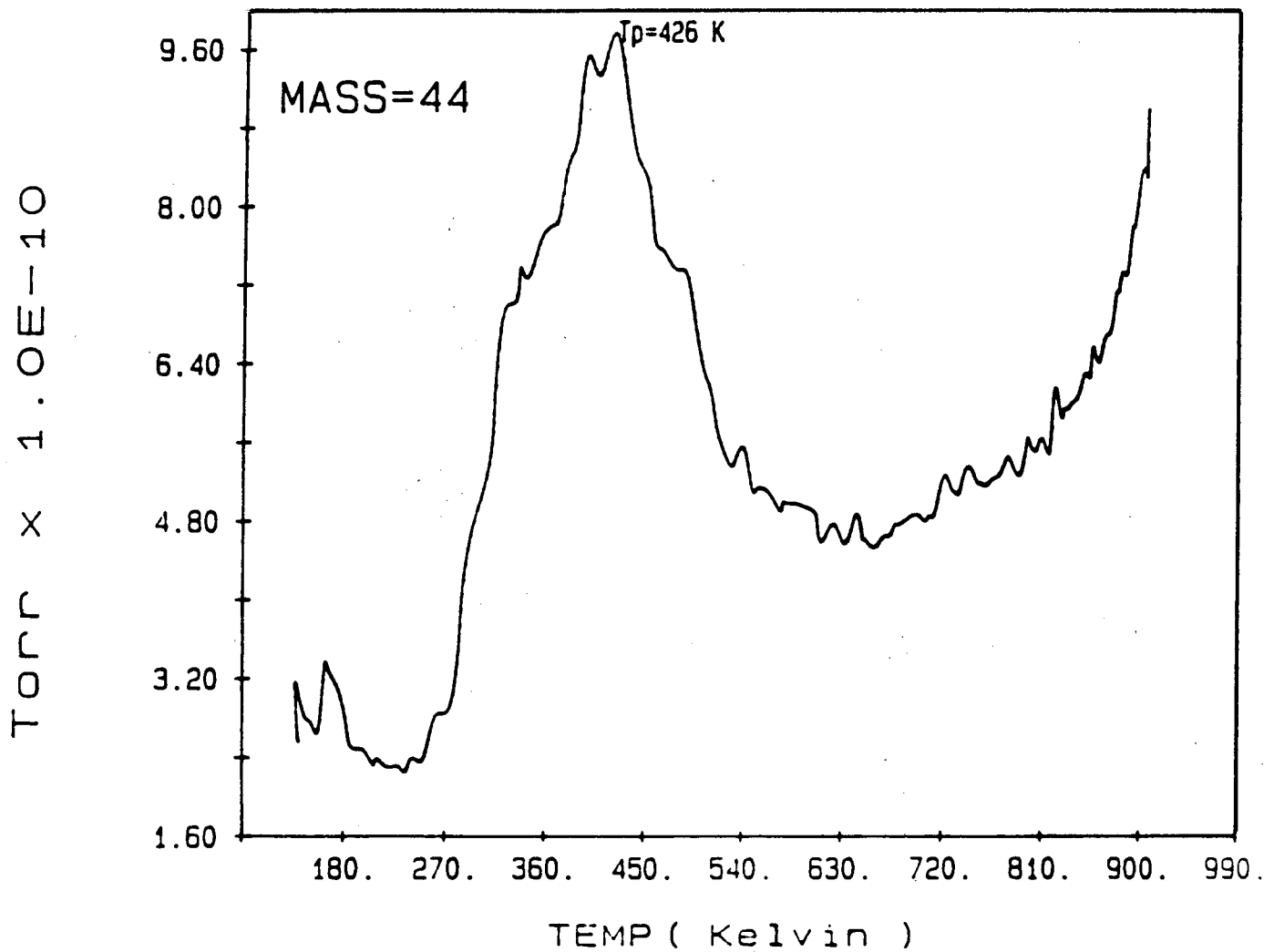

Fig. 4. Mass 44 TDS of 180 L of O_2 adsorbed on Ag(111) at -186°C. Heating rate = 4.3 K • s^{-1}.

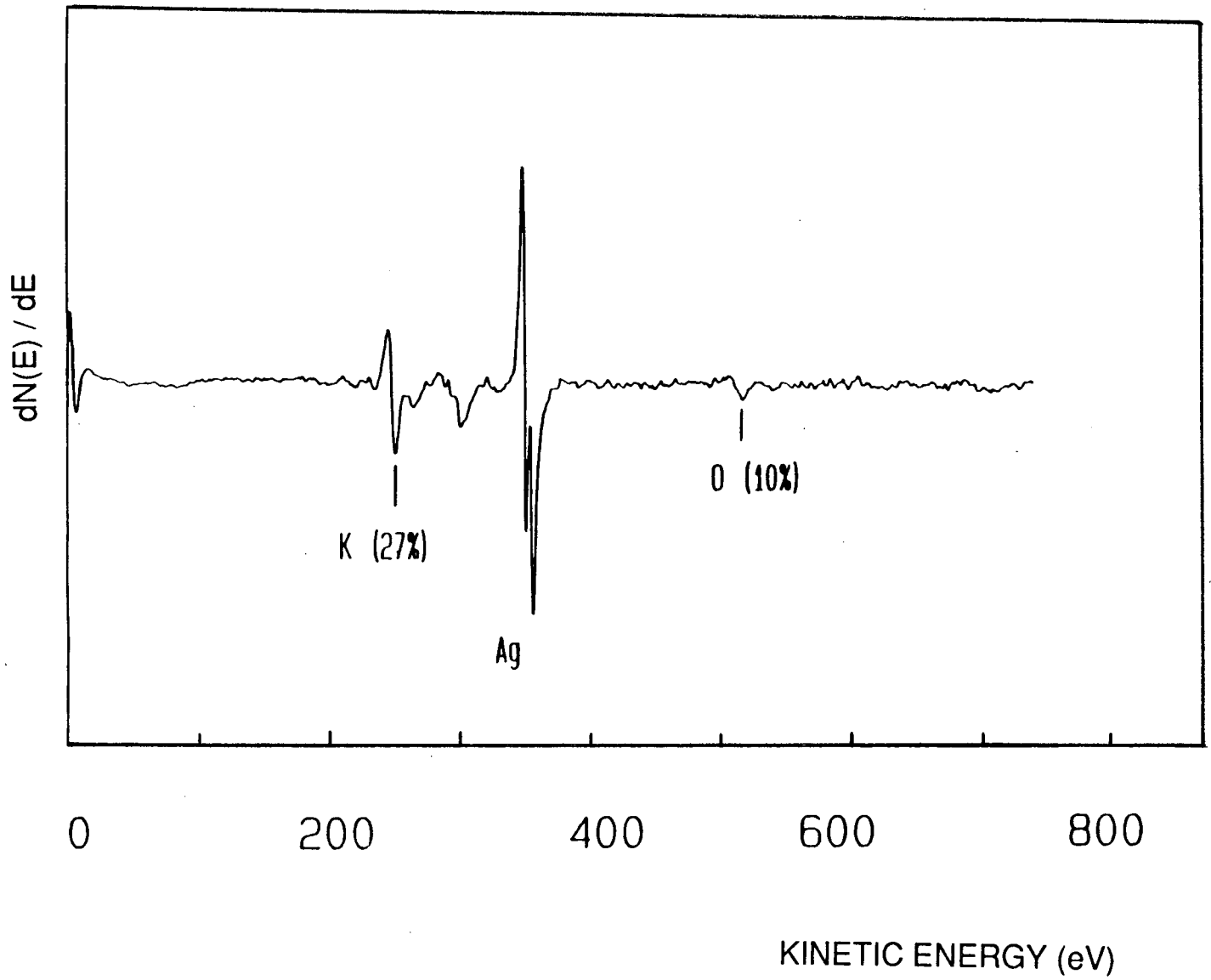

Fig. 5. AES of surface containing 27% K and 10% oxygen.

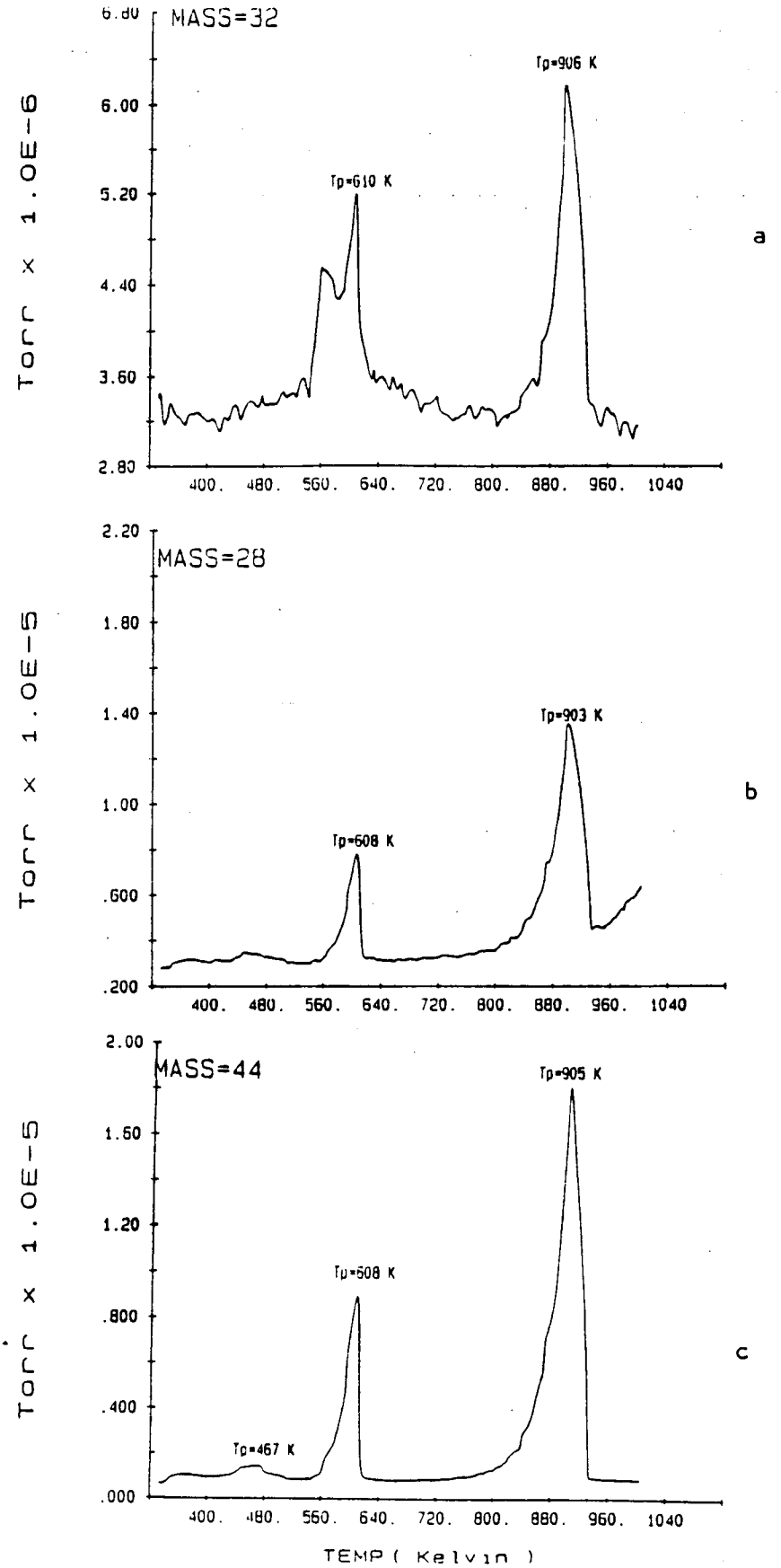

Fig. 6. TDS spectra of surface described in caption Fig. 5. a. Mass 32, b. Mass 28, and c. Mass 44.

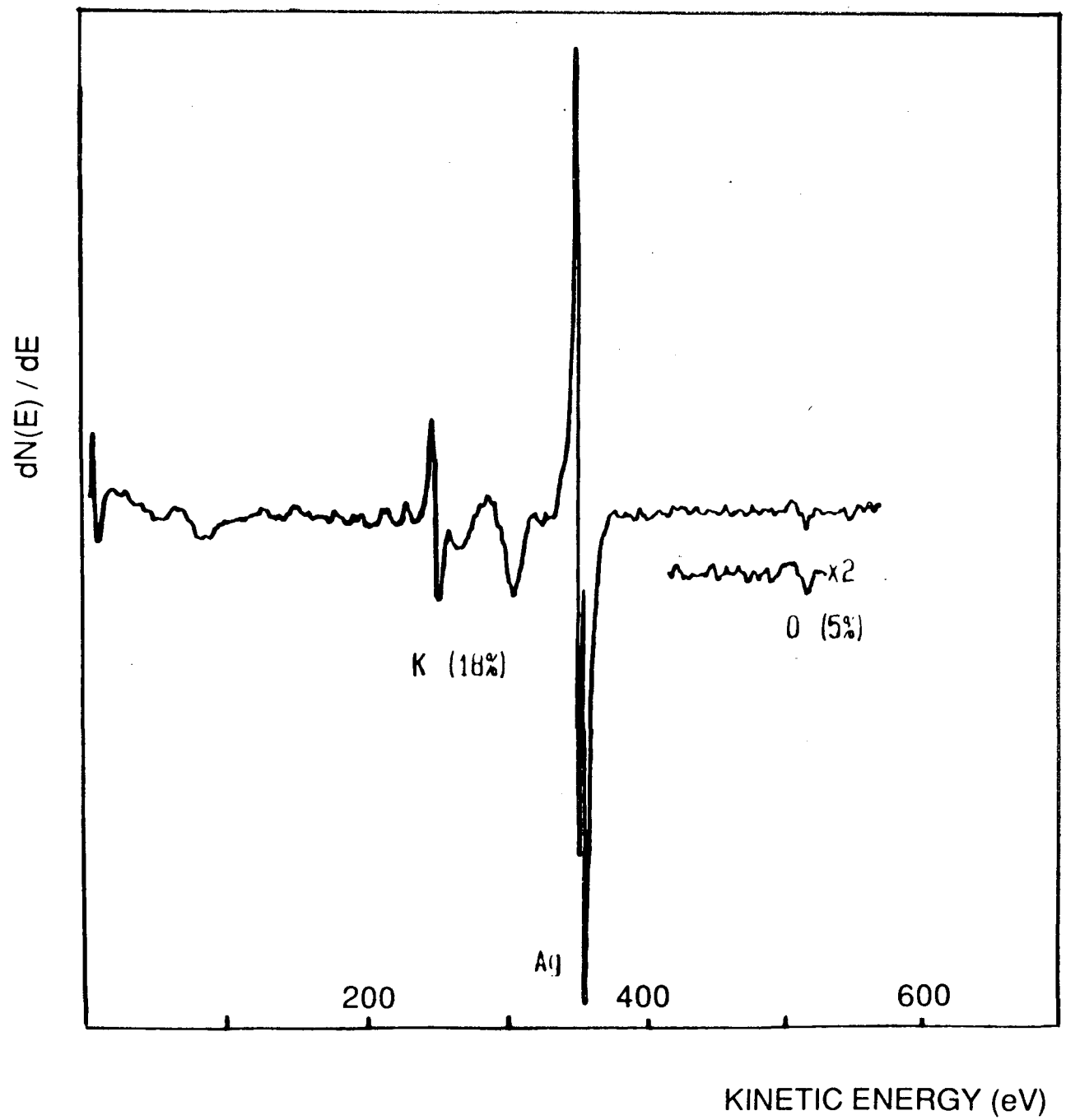

Fig. 7. AES of K / Ag(111) surface dosed with 200 L CO.

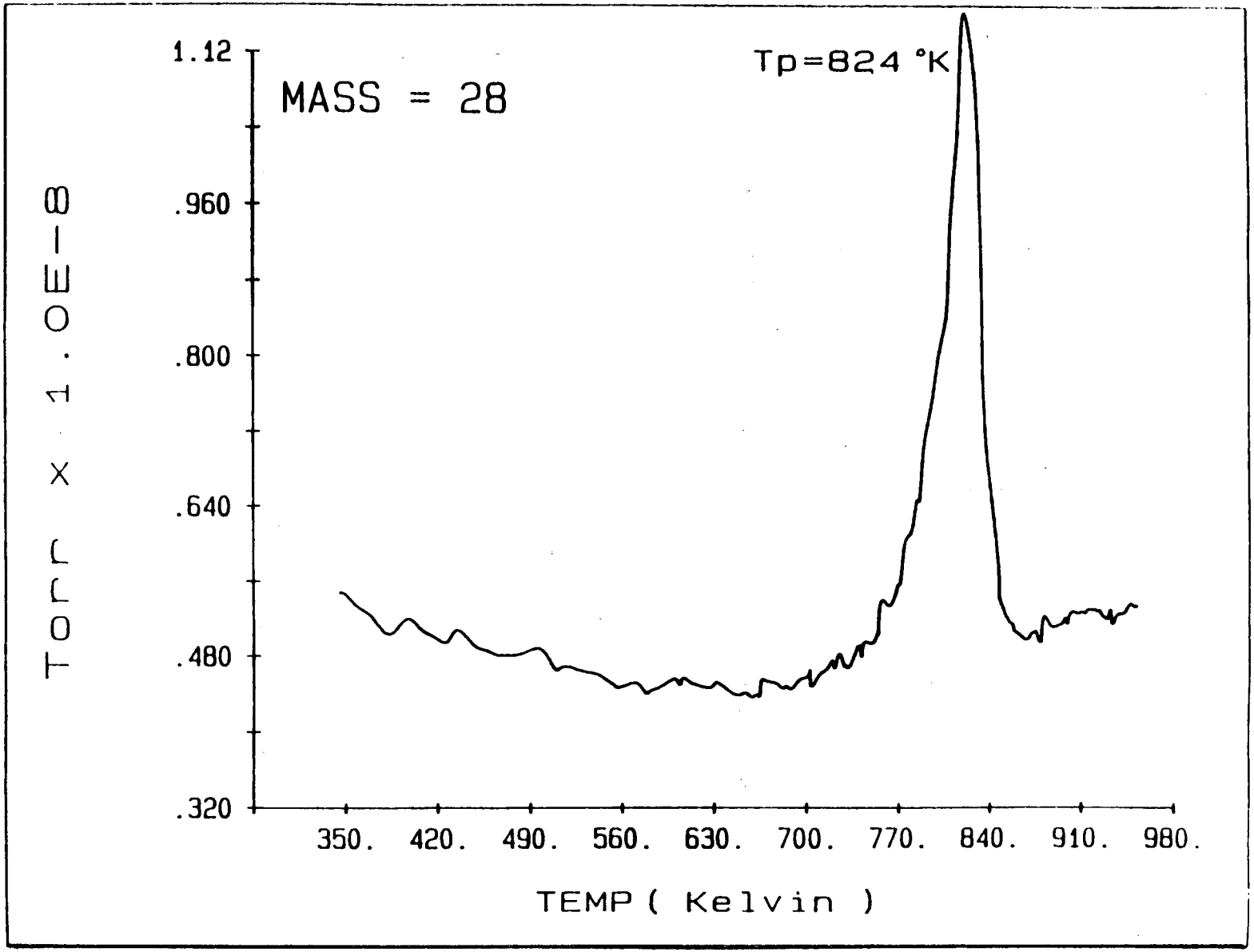

Fig. 8. CO-TDS of surface described in caption Fig. 7.

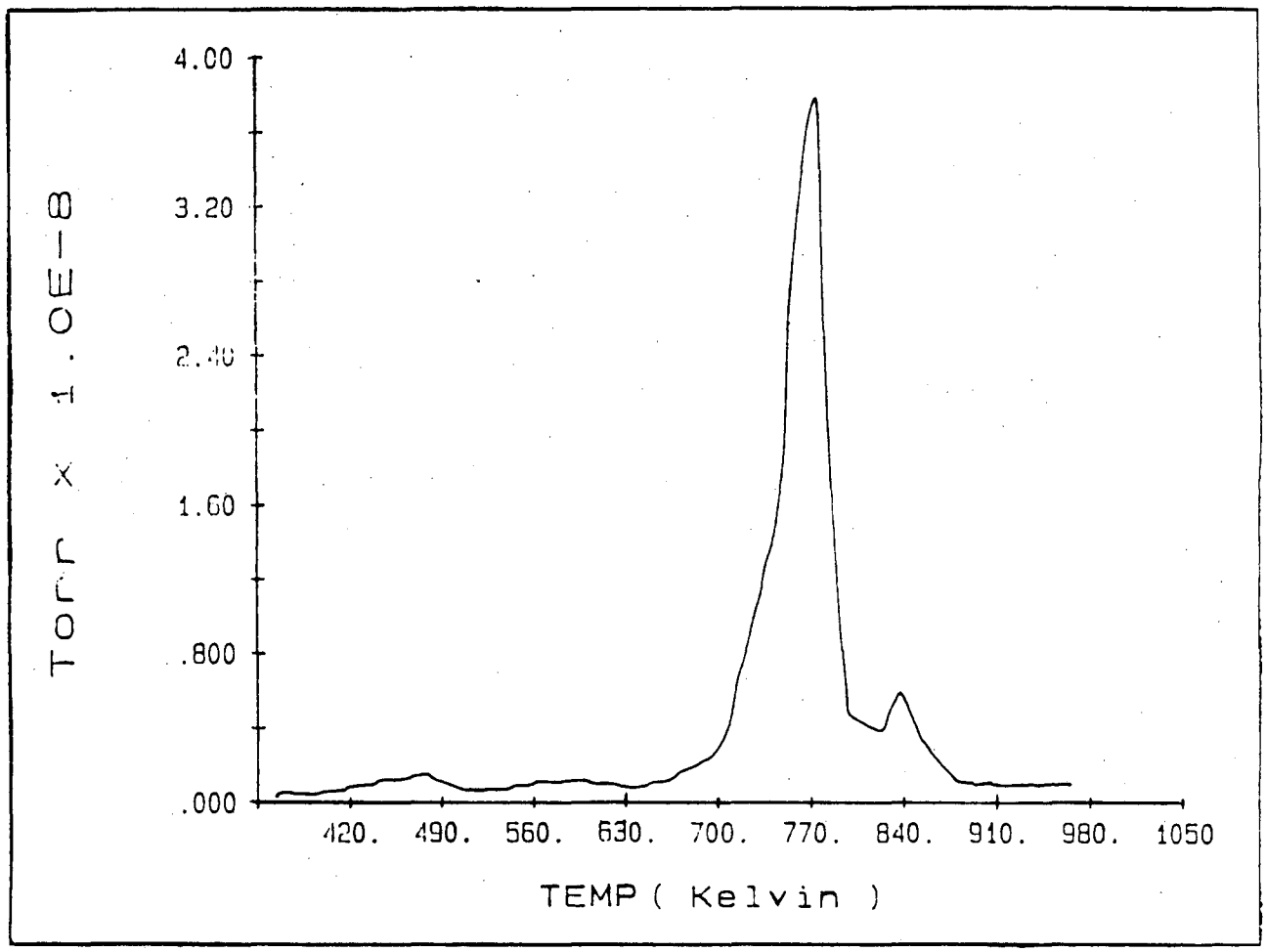

Fig. 9. Thermal desorption spectra of a surface containing 14% K exposed to 0.5 L CO_2. Heating rate: 6 K • s^{-1}.

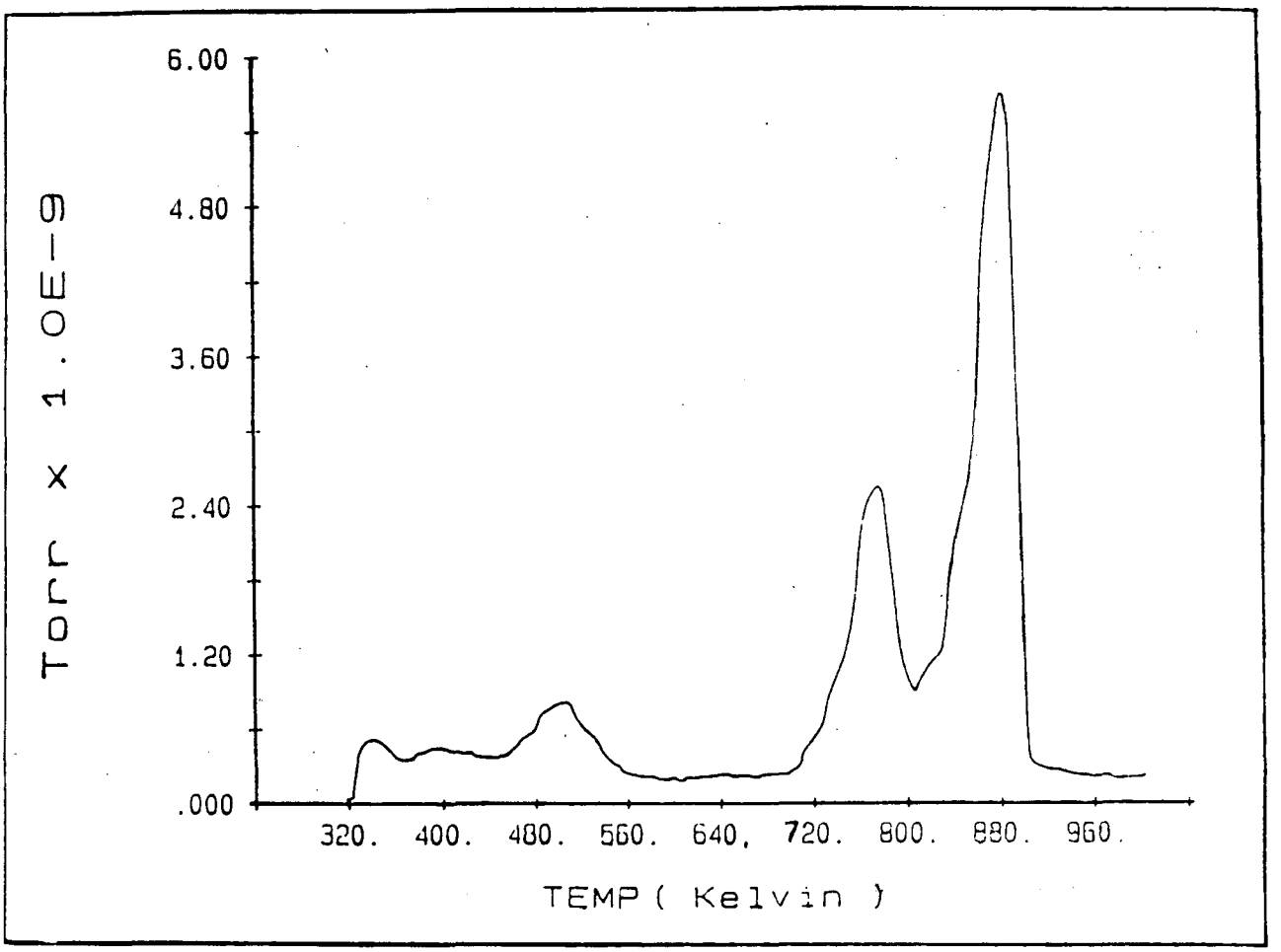

Fig. 10. Thermal desorption spectra of a surface containing 18% K exposed to 60 L CO_2. Heating rate: 6 K • s^{-1}.

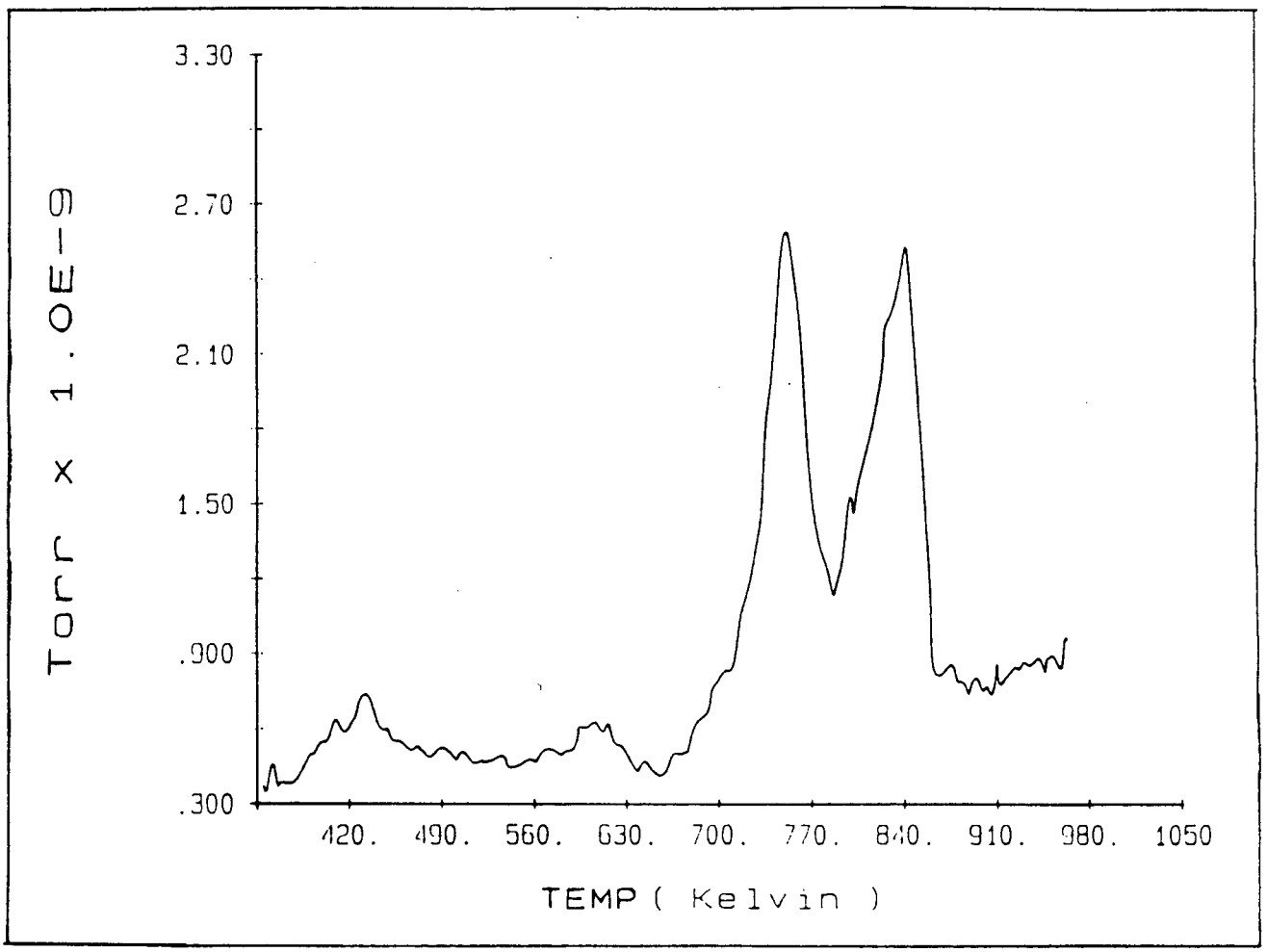

Fig. 11. Thermal desorption spectra of a surface containing 9% K exposed to 0.25 L CO_2. Heating rate: 6 K • s^{-1}.

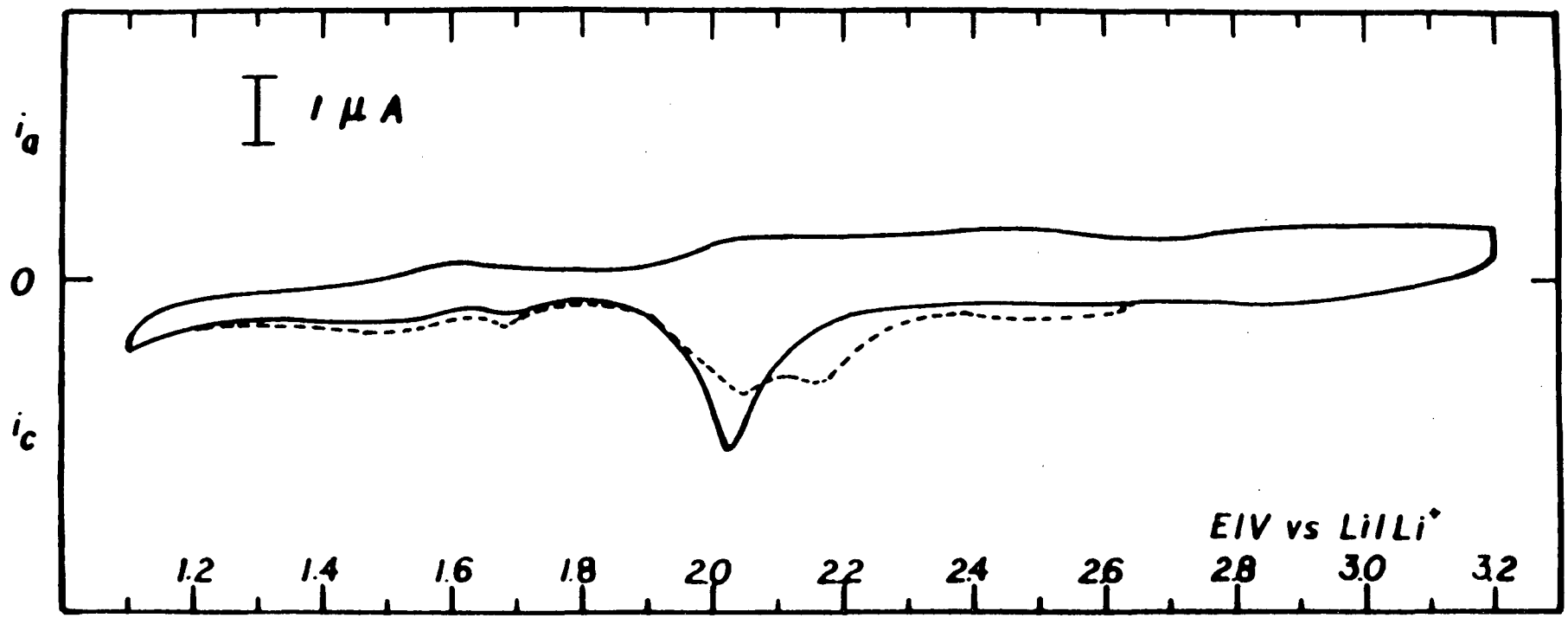

Fig. 12. Cyclic voltammogram of Ag(111) in 2mM TBAP / PC solution.
$\nu = 10\ mV \cdot s^{-1}$. -----: first cycle. ——— : subsequent cycles.

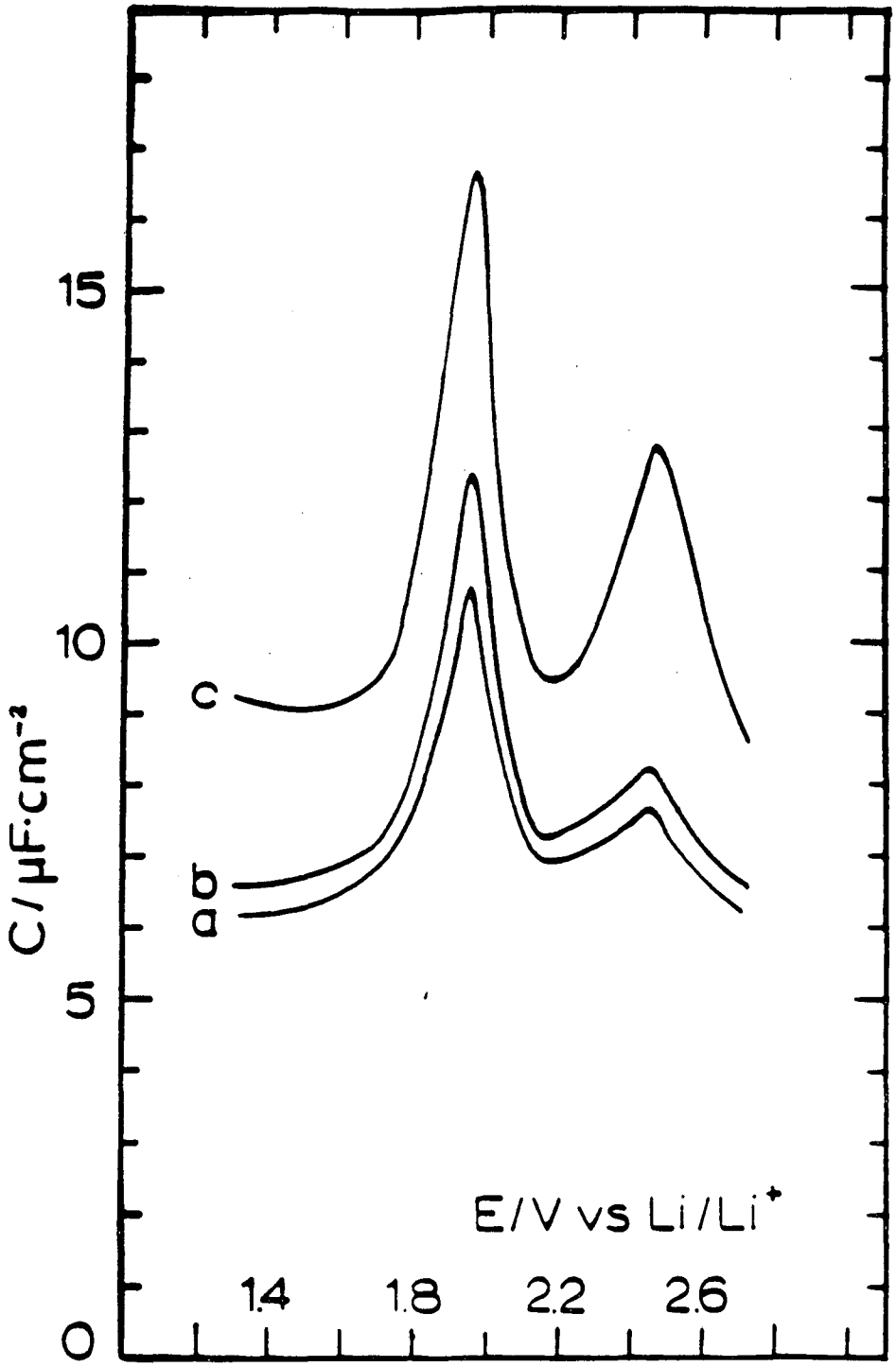

Fig. 13. C vs. E curves for Ag(111) in TBAP / PC solutions: a. 8mM; b. 10mM c. 50 mM. ν =5 mV • s^{-1}. AC signal: Amplitude = 5 mV, f = 40 Hz.

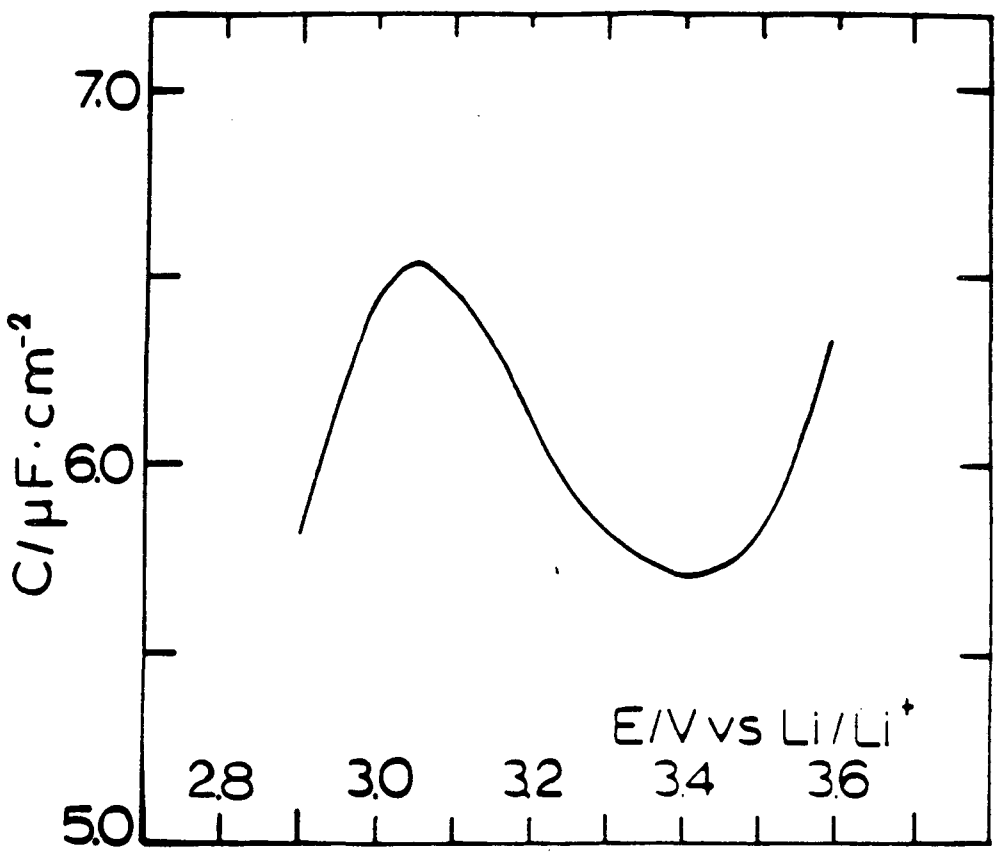

Fig. 14. C vs. E curves for Au(111) in 0.01 M TBAP / PC solution. $\nu = 10\ mV \cdot s^{-1}$. AC signal: Amplitude = 5 mV, f = 20 Hz.

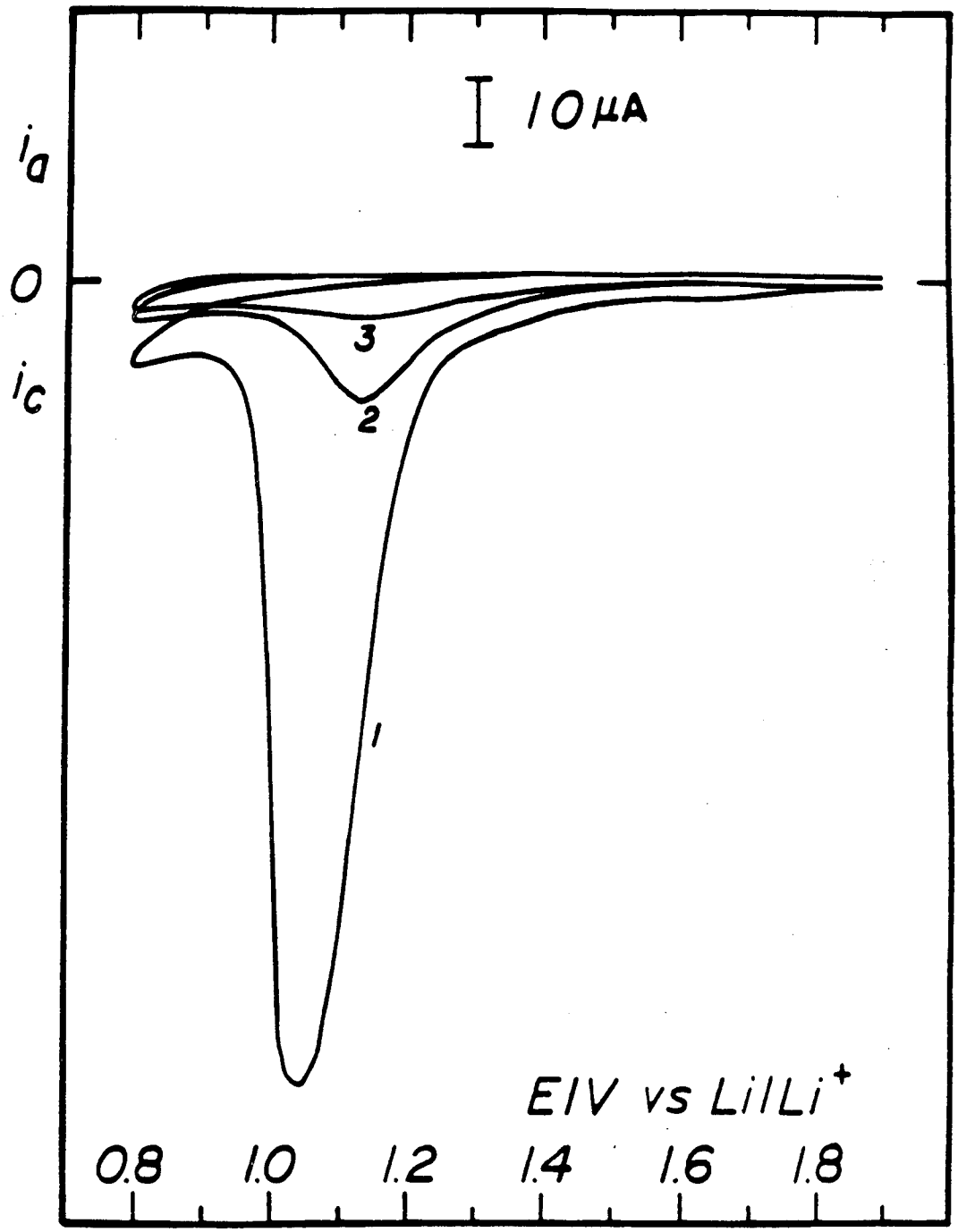

Fig. 15. Cyclic voltammogram of Ag(111) in 0.1 M $LiClO_4$ / PC solution. $\nu = 10\ mV \cdot s^{-1}$. 1. first, 2. second, and 3. third cycle.

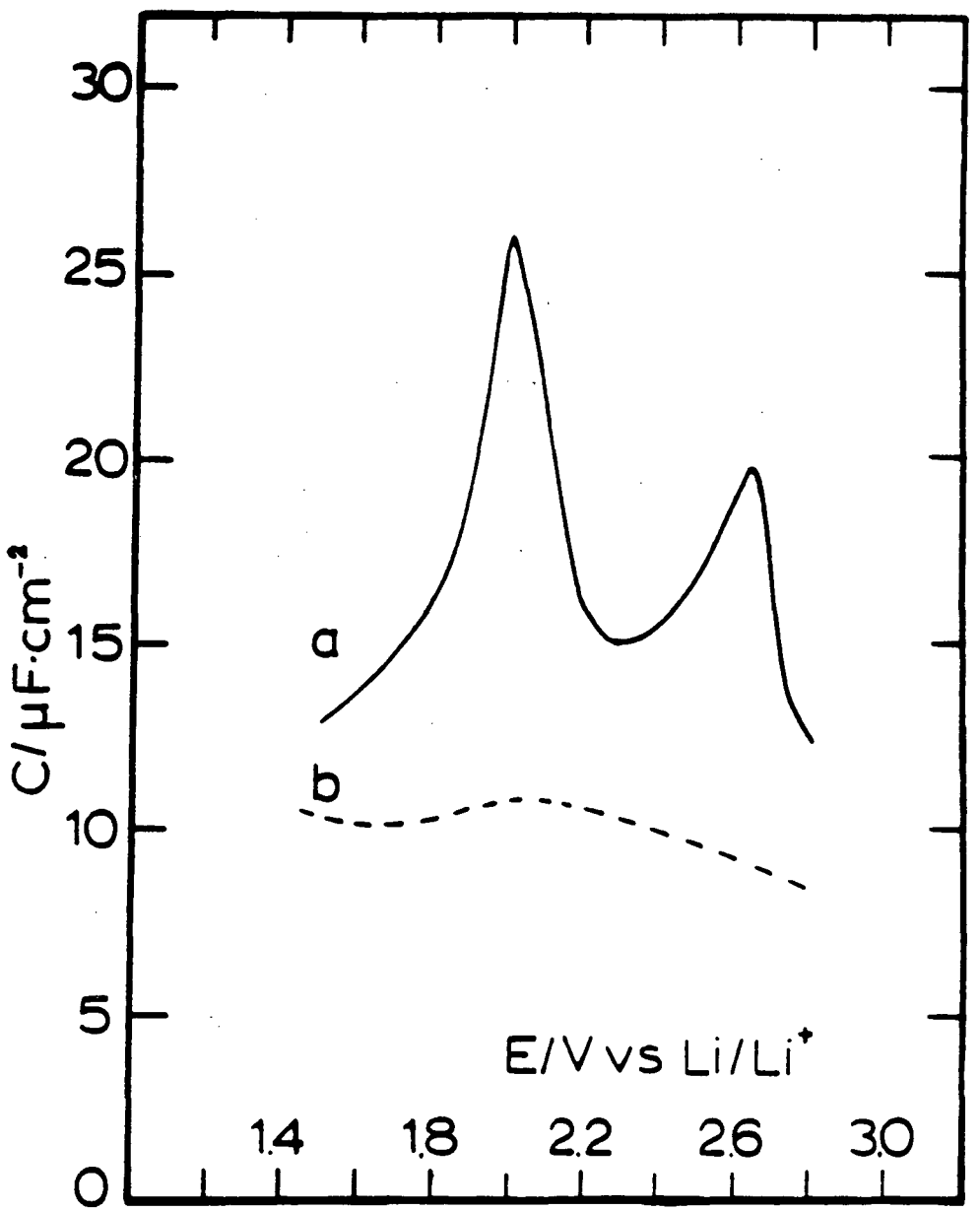

Fig. 16. C vs. E curves for Ag(111) in 50 m<u>M</u> $LiClO_4$ solution, before (a) and after (b) excursion to negative region (0.8 V vs. Li / Li^+).

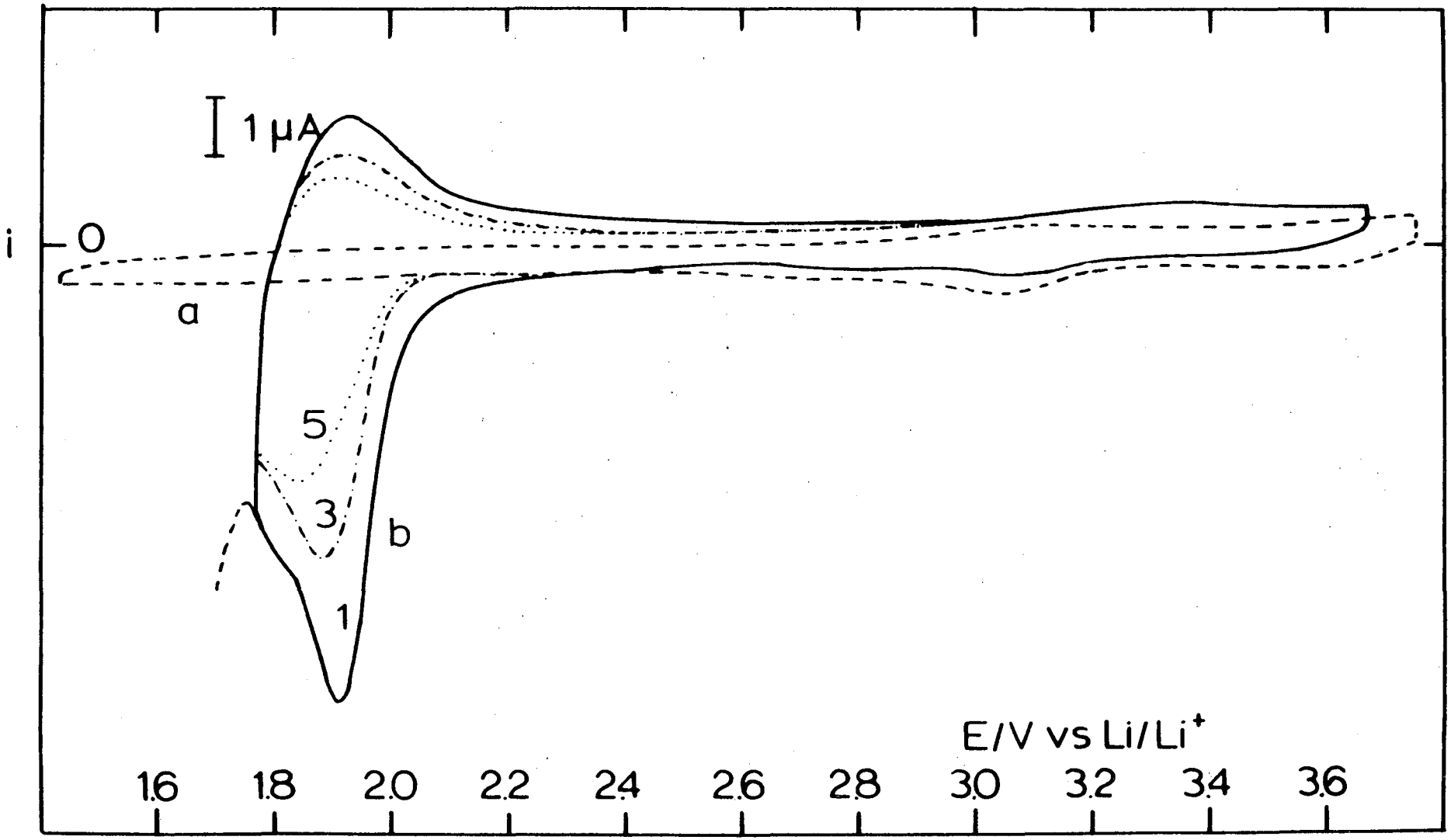

Fig. 17. Cylcic voltammogram of Au(111) in PC solution containing:
a. 0.01 M TBAP
b. 0.01 M $LiClO_4$
$\nu = 10\ mV \cdot s^{-1}$. Number represents the cycle sequence.

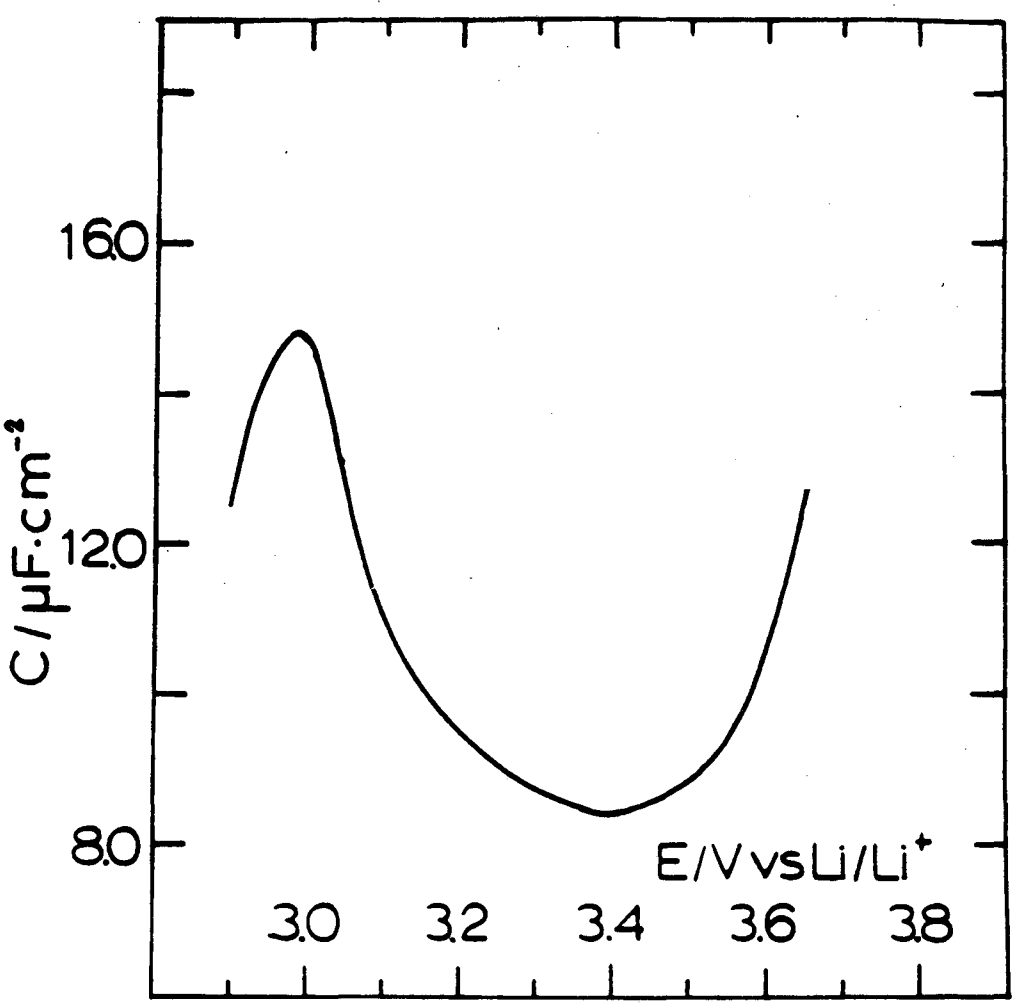

Fig. 18. C vs. E curves for Au(111) in 0.01 M $LiClO_4$ / PC solution. $\nu = 10\ mV \cdot s^{-1}$. AC signal: Amplitude = 5 mV, f = 20 Hz.

LAWRENCE BERKELEY LABORATORY
TECHNICAL INFORMATION DEPARTMENT
UNIVERSITY OF CALIFORNIA
BERKELEY, CALIFORNIA 94720